J. of KOSOMBE
Vol. 19, No. 3, 225-232, 1998

# 무정형 실리콘(a-Si : H) 디지털 X-선 영상기기의 개발을 위한 Monte Carlo 컴퓨터 모의실험연구

이 형 구·신 경 섭

가톨릭대학교 의과대학 의공학교실

*(1997년 12월 22일 접수, 1998년 4월 3일 채택)*

# Monte Carlo Studies on an Amorphous Silicon (a-Si : H) Digital X-Ray Imaging Device

H. K. Lee, K. S. Shinn

Department of Biomedical Engineering
Medical College, Catholic University of Korea, Seoul

*(Received December 22, 1997, Accepted April 3, 1998)*

**요 약** : 무정형 실리콘을 기반으로 한 X-선 영상기기에 대한 Monte Carlo 시뮬레이션 결과를 기술하였다. 무정형 실리콘 X-선 영상기기의 특성을 조사하고 최적의 설계변수들을 제공하기 위하여 Monte Carlo 시뮬레이션을 수행하였다. 본 연구의 목적에 맞도록 Monte Carlo simulation codes를 개발하였고, X-선 최대전압, 알루미늄 필터 두께, CsI(Tl) 두께, 그리고 무정형 실리콘 광다이오우드 픽셀 크기들을 변화시키면서 무정형 실리콘 X-선 영상기기의 계측 효율과 해상도의 변화를 연구하였다. 60kVp~120kVp의 X-선에 대하여, CsI(Tl)의 두께가 300$\mu$m~500$\mu$m일 때 계측효율은 70%~95% 였고 에너지 흡수효율은 40%~70%였다. 시뮬레이션 결과로부터, 무정형 실리콘 픽셀크기와 CsI(Tl) 두께가 해상도를 결정하는 가장 주된 요소임이 밝혀졌다. 본 연구에서 개발한 시뮬레이션을 사용하여 감도와 해상도를 최적화할 수 있는 적절한 픽셀 크기와 CsI(Tl) 두께를 찾아낼 수 있었다.

**Abstract** : Results of Monte Carlo simulations on amorphous silicon based x-ray imaging arrays are described. In order to investigate the characteristics of amorphous silicon x-ray imaging devices and to provide the optimum design parameters, Monte Carlo simulations were performed. Monte Carlo simulation codes for our purpose were developed and various combinations of x-ray peak voltages, aluminum filter thicknesses, CsI(Tl) thicknesses, and amorphous silicon photodiode pixel sizes were tested in connection with detection efficiency and spatial resolution of the amorphous silicon based x-ray imager. With usual CsI(Tl) thickness of 300$\mu$m~500$\mu$m, detection efficiency was in the range of 70%~95% and energy absorption efficiency was in the range of 40%~70% for 60kVp~120kVp x-rays. From the simulations it was found that amorphous silicon pixel size and CsI(Tl) thickness were the most important parameters which determine the resolution of the imager. By use of our simulation results we could provide proper combinations of CsI(Tl) thicknesses and pixels sizes for optimum sensitivity and resolution.

**Key words** : amorphous silicon, digital x-ray imager, Monte Carlo simulation, CsI(Tl)

## INTRODUCTION

Hydrogenated amorphous silicon (a-Si:H) is a relatively new material with a short history compared to other semiconductor materials. This material, however, has been investigated extensively in many groups around the world in connection with its various applications. Due to its ability of being deposited on a large area substrate with any geometry and its high radiation hardness, amorphous silicon

통신저자 : 이형구, (137-040) 서울시 서초구 반포동 505 가톨릭의과학연구원 생체의공학연구소
Tel. (02)590-2415, Fax. (02)590-2425

has also been investigated as a material for large area radiation imaging devices[1-5]. Though it is still under development, amorphous silicon radiation imaging arrays may replace many of the conventional imaging devices such as x-ray films and image intensifying tubes in the near future.

The radiation detectors made from amorphous silicon usually have p-i-n structures in sandwich type. Amorphous silicon p-i-n diodes can be fabricated in small pixels, making two dimensional imaging possible. For x-ray imaging, amorphous silicon pixel detector arrays are usually in direct contact with a scintillating layer which converts the absorbed x-ray energy in the scintillator into many visible photons, hence amplifying the output signals of the amorphous silicon photodiodes compared to the direct x-ray detection by themselves. As the mean free path of the visible light is short in the amorphous silicon, a thin i-layer can be used. A 1 $\mu$m thick i-layer can absorb about 96% of the light incident on the p-i-n diode[6]. The thickness of the scintillator is usually less than 500 $\mu$m for x-ray detection[1,4,5]. Choice of the scintillator depends on specific requirements of detection such as signal size, speed and spatial resolution. There are many candidates of scintillator which can be coupled to amorphous silicon photodiodes. These include CsI(Tl), CsI(Na), $CdWO_4$, ZnS(Ni) and $Gd_2O_2$S:Tb. Among these, CsI(Tl) has drawn much attention due to its high light yield (about 52,000 photons/1 MeV absorbed energy) and a good emission spectrum that matches the amorphous silicon photodiode quantum efficiency spectrum[4,7,8].

There are a few characteristics which represent the performance of amorphous silicon based x-ray imaging arrays. These include detection efficiency, spatial resolution, linearity of pixel response, image lag, frame rate and noise, which determine the operation conditions of the imaging arrays. According to the experimental results of other workers, the linearity, image lag, frame rate and noise characteristics were found to be acceptable and are still being improved[2,4,5,9-12]. Detection efficiency and spatial resolution are usually determined by the x-ray energy and the geometric condition such as scintillator thickness, amorphous silicon pixel size. These properties can be measured experimentally, however it costs much time, budget and effort to investigate the whole combinations of various parameters by experiments. We, therefore, generated Monte Carlo simulation codes in order to investigate the effect of x-ray energy, filter thickness, scintillator thickness, and pixel size on the detection efficiency and resolution. The results from the simulations and the design parameters obtained from these results are described in this paper.

## METHODS

The Monte Carlo simulation codes for our study were made using C++ language. The material data used in the codes were obtained from Evaluated Photon Data Library (EPDL) of Lawrence Livermore National Laboratory[13].

The random number generator was adopted from Park and Miller's Minimal Standard generator with an additional shuffle[14]. Tungsten target was used for x-ray sources and the x-rays from the target were filtered by various thickness of aluminum filter. In the simulations both the bremsstrahlung and characteristic x-rays were made to be generated from the tungsten target, but the intensities of the characteristic x-rays were not precisely simulated, because the importance of the characteristic x-rays relative to the bremsstrahlung spectrum in diagnostic x-rays is not great due to their small contribution to the total produced energy[15].

CsI(Tl) was used as the scintillator and its thickness was varied in the simulations. The visible photons, which are generated by interactions of x-rays with CsI(Tl), were isotropically emitted and their generation number was assumed to follow a normal distribution with a mean value of $5.2\times10^4\cdot E_x$ photons, where $E_x$ is the absorbed x-ray energy expressed in MeV. The amorphous silicon p-i-n diode pixel pitch was varied in the simulations and this effect on the resolution was analyzed by means of modulation transfer functions(MTF) which were obtained from line spread functions(LSF). The quantum absorption efficiency of amorphous silicon pixel detector was assumed to be 70%[3].

Only photoelectric effect, characteristic x-ray generation and Compton scattering were considered as the x-ray interactions in materials, since other interactions are relatively negligible in diagnostic x-ray energy range. The position of the interaction and the direction of the scattered photons were calculated based on the cross section data from EPDL. Details of these calculations are as follows.

### 1. Next Interaction Position

An X-ray either from the source or Compton scattering event will have an interaction inside the medium or escape from it. In order to find which is the case, the distance

from the entrance position of the X-ray or previous scattering position to the next interaction position is needed. When an X-ray is traveling a distance s, the probability, $p(s)ds$, of having an interaction between $s$ and $s+ds$ is

$$p(s)ds = \Sigma_t(E)e^{-\Sigma_t(E)s}ds \tag{1}$$

where $\Sigma_t(E)$ is the total linear attenuation coefficient of a photon with the energy $E$. The integration of $p(s)$ from s= 0 to infinity gives unity, hence $p(s)$ is a probability density function (PDF) and the cumulative distribution function (CDF) corresponding to this PDF is

$$P(s)=\int_0^s p(s')ds' = 1-e^{-\Sigma_t(E)s}\ . \tag{2}$$

Then, using the inverse distribution method[16], s, which is the traveling distance of the photon from the last event to the next interaction, can be obtained by

$$s=P^{-1}(\xi)=-\frac{1}{\Sigma_t}\ln, \qquad 0<\xi\leq 1, \tag{3}$$

where $\xi$ is a random number which is uniform between 0 and 1. If a photon at a position $r_1(x_1, y_1, z_1)$ is heading to the direction of $\omega(\omega_x, \omega_y, \omega_z)$, then the position $r_2(x_2, y_2, z_2)$ where the photon will have an interaction with the medium is

$$\begin{aligned} x_2 &= x_1 + s\omega_x \\ y_2 &= y_1 + s\omega_y \\ z_2 &= z_1 + s\omega_z \end{aligned} \tag{4}$$

where $\omega_x$, $\omega_y$ and $\omega_z$ are the x, y and z components of the directional unit vector $\omega$ and s is obtained from Eq. (3). If $r_2$ is out of the medium, then that photon does not have an interaction in the corresponding medium any more.

### 2. Selection of Interaction Type

Whenever an X-ray interaction position is given in a medium, the type of the interaction is determined by the following simple rejection technique. First, select a random number, $\xi$. If $\xi$ is smaller or equal to $\Sigma_p(E)/\Sigma_t(E)$, where $\Sigma_p(E)$ and $\Sigma_t(E)$ is the linear attenuation coefficient for photoelectric absorption and total interactions, respectively, then this photon encounters a photoelectric absorption interaction on that position. Otherwise, it has a Compton scattering event on that position.

### 3. Direction of Compton Scattered X-Ray

When an X-ray is Compton scattered it loses part of its energy and deflected. Therefore a new direction and a new energy of the scattered photon should be computed, which can be done using the angular dependent cross section of the Compton scattering. The Klein-Nishina's formula for the differential cross section of the Compton scattering is [16]

$$\frac{d\sigma_c(\alpha,\theta)}{d\Omega}=\gamma_o^2\left[\frac{1}{1+\alpha(1-\cos\theta)}\right]^3\left(\frac{1+\cos^2\theta}{2}\right) \left\{1+\frac{\alpha^2(1-\cos\theta)^2}{(1+\cos^2\theta)[1+\alpha(1-\cos\theta)]}\right\}, \tag{5}$$

where, $\Omega$ is the solid angle, $\alpha$ is the energy of the incident photon in electric rest mass energy unit, $r_o$ is the classical radius of the electron and $\theta$ is the deflection angle of the scattered photon. The total cross section, $\sigma_c(\alpha)$ is obtained by integration of Eq. (5) and is expressed as

$$\sigma_c(\alpha)=2\pi\gamma_o^2\left\{\frac{1+\alpha}{\alpha^2}\left[\frac{2(1+\alpha)}{1+2\alpha}-\frac{\ln(1+2\alpha)}{\alpha}\right] +\frac{\ln(1+2\alpha)}{2\alpha}-\frac{1+3\alpha}{(1+2\alpha)^2}\right\}. \tag{6}$$

The cross sections in Eq. (5) and (6) are independent of the atomic numbers of the elements which constitute the given medium. Hence the angle of scattering can be selected by the same procedure for any medium. The PDF to be sampled can be expressed as

$$p(\alpha,\theta)=\frac{1}{\sigma_c(\alpha)}\frac{d\sigma_c(\alpha,\theta)}{d\Omega}. \tag{7}$$

Now, as the PDF is known, selection of the scattered angle, $\theta$, is possible. There are many procedures to select $\theta$ from Eq. (7), including the rejection technique, inverse CDF method and direct sampling etc. Among these, the rejection method proposed by Kahn was used, which is very efficient for low energies (E≤1.4 MeV)[17].

Once $\theta$ is selected, the directional unit vector $\omega'(\omega'_x, \omega'_y, \omega'_z)$ of the scattered photon can be found by following equations.

For $-1 < \omega_z < 1$,

$$\omega'_x=\sqrt{\frac{1-\mu^2}{1+\omega_z}}[\omega_y\cos\phi+\omega_x\omega_z\sin\phi]+\omega_x\mu,$$

$$\omega'_y = \sqrt{\frac{1-\mu^2}{1+\omega_z^2}}\left[-\omega_x\cos\phi+\omega_y\omega_z\sin\phi\right]+\omega_y\mu, \quad (8a)$$

$$\omega'_z = \sqrt{(1-\omega_z^2)(1-\mu^2)}\sin\phi+\omega_z\mu$$

And, for $\omega_i = \pm 1$,

$$\omega'_x = \sqrt{1-\mu^2}\cos\phi,$$

$$\omega'_y = \sqrt{1-\mu^2}\sin\phi,$$

$$\omega'_z = \omega^z\mu,$$

where, $\Phi$ is the azimuthal angle and $\mu$ is $\cos\theta$. As the distribution of the scattered photons across the azimuthal angle is uniform, $\Phi$ can be selected by $\Phi = 2\pi\xi$, where $\xi$ is a random number.

## RESULTS AND DISCUSSION

### 1. X-Ray Energy Spectrum from Target

Simulated x-ray energy spectra from tungsten target with various peak voltages are shown in Fig. 1. For photon energies greater than 69 keV, the K-beta lines are shown. As the EPDL table do not provide the K-alpha line data, we could not generate the K-alpha lines. The whole characteristic x-ray photons can be neglected, however, since the tungsten characteristic x-rays constitute only a small fraction of the total energy[15].

### 2. Filtered X-Ray Energy Spectrum

X-ray energy spectra after aluminum filtration are shown in Fig. 2. The spectra in Fig. 1 were used as the input x-rays. 1.5 mm aluminum was used for 60 kVp x-rays and 2.5mm was used for the other x-rays. It is shown that the low energy portion of the input x-rays are significantly reduced by the filter. These x-ray energy spectra were in good agreement with the measurements[18], providing thus the reliability of our simulation results. The average energy of the filtered x-rays are listed in Table 1. The filter thickness effect on the average energy for the case of 100 kVp x-rays (0.8 keV increase per 0.5 mm addition) is also shown in this table.

### 3. Detection Efficiency

The quantum detection efficiency, ratio of detected photon numbers to incident photon numbers, of amorphous silicon

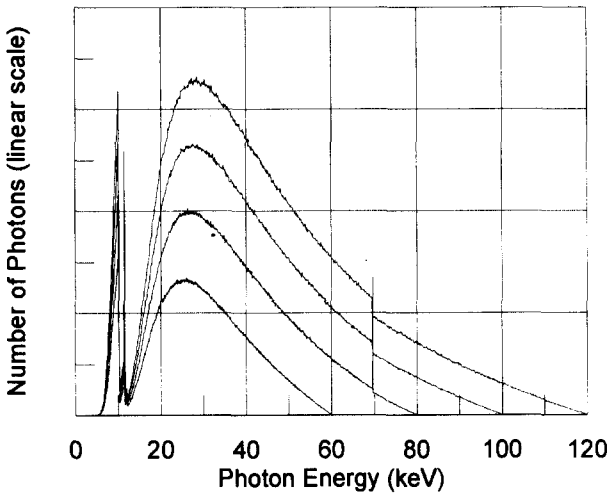


그림 1. 텅스텐 타겟으로부터 발생되는 X-선의 에너지 스펙트럼. 각 스펙트럼의 크기는 구별을 위하여 조절되었음

Fig. 1. X-ray energy spectra from tungsten target. The scale for each spectrum is adjusted for easy differentiation

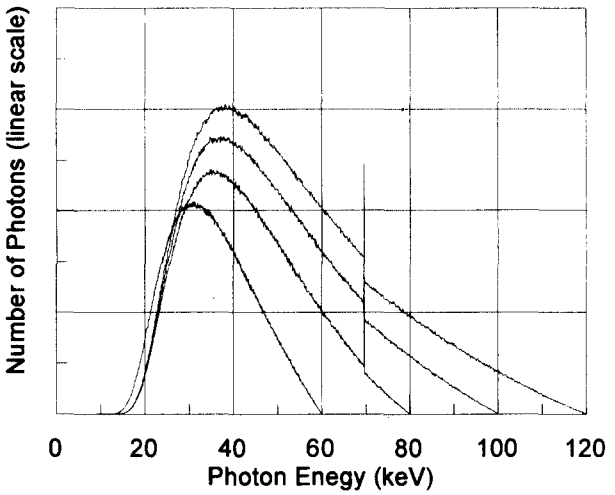


그림 2. 알루미늄 필터를 투과한 X-선의 에너지 스펙트럼. 그림 1의 스펙트럼이 입력 X-선으로 사용되었다. 각 스펙트럼의 크기는 구별을 위하여 조절되었음

Fig. 2. Aluminum filtered x-ray energy spectra. The spectra in Fig. 1 were used as the input x-rays. The scale for each spectrum is adjusted for easy differentiation

표 1. 알루미늄 필터를 투과한 X-선의 평균 에너지

Table 2. Average energies of aluminum filtered x-rays

| Peak Energy | Al Filter Thickness | Average Energy |
|---|---|---|
| 60 keV | 1.5 mm | 34.9 keV |
| 80 keV | 2.5 mm | 42.8 keV |
| 100 keV | 2.5 mm | 48.2 keV |
| 100 keV | 3.0 mm | 49.0 keV |
| 100 keV | 3.5 mm | 49.8 keV |
| 120 keV | 2.5 mm | 53.2 keV |

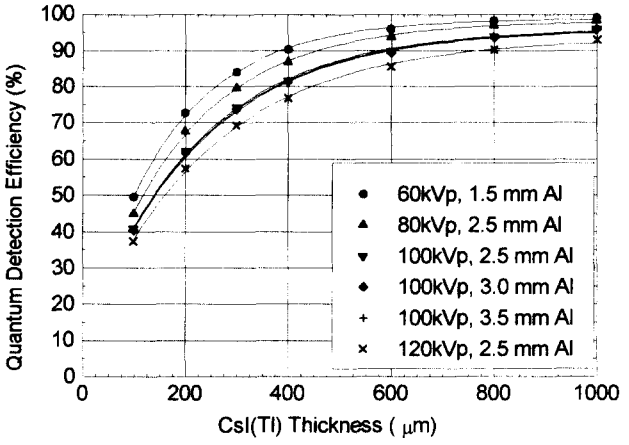


그림 3. CsI(Tl)의 광자계측효율
Fig. 3. Quantum detection efficiency of CsI(Tl)

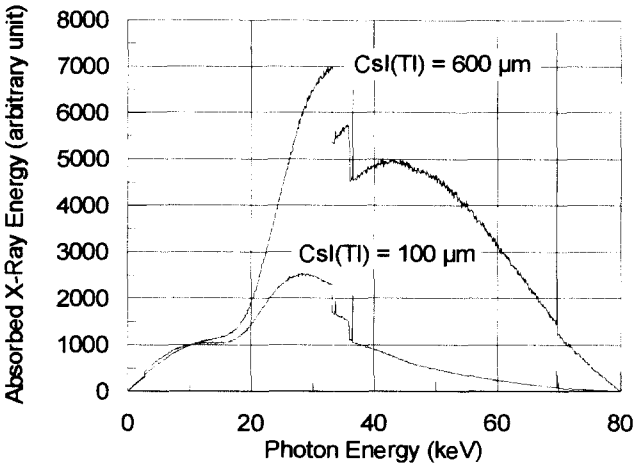


그림 4. 그림 2의 80 kVp X-선에 대한 100$\mu$m와 600$\mu$m 두께의 CsI(Tl)의 에너지 흡수 스펙트럼. 33.70 keV와 36.52 keV에서의 피크는 텅스텐 characteristic X-선의 photoelectric 흡수 후에 발생하는 세슘과 요오드의 escape 피크임
Fig. 4. Absorbed x-ray energy spectra in 100$\mu$m and 600$\mu$m thick CsI(Tl) when the same 80 kVp x-ray in Fig. 2 is incident. Peaks at 33.70 keV and 36.52 keV are the escape peaks of cesium and iodine, respectively, which occur following photoelectric absorption of tungsten characteristic x-rays

based x-ray imager is dependent on scintillator thickness and input x-ray energy. Fig. 3 shows the quantum detection efficiency of CsI(Tl) for various x-rays. With a CsI (Tl) thickness of 100$\mu$m, the quantum detection efficiency is 50% for 60 kVp x-rays and 37% for 120 kVp x-rays. For the usual CsI(Tl) thickness of 300$\mu$m~500$\mu$m, the quantum detection efficiency is in the range of 70%~95% for diagnostic beams. Thickening of filters slightly decrease the absorption efficiencies of CsI(Tl) because of x-ray hardening as shown in Table 1 and Fig. 3 for the case of 100 kVp, which is, however, only 0.7%~0.9% decrease per 1 mm addition of filter thickness.

The light output from CsI(Tl) is directly dependent on the x-ray energy deposition in it, hence the final signal size of the amorphous silicon detectors depends on the energy absorption efficiency (ratio of absorbed energy to total energy of incident photons) of CsI(Tl). The energy absorption efficiency (EAE) and the quantum detection efficiency (QDE) is related by $EAE=QDE\cdot E_{D,avg}/E_{I,avg}$, where $E_{D,avg}$ and $E_{I,avg}$ is the average energy of detected photons and incident photons, respectiely. Fig. 4 shows examples of the energy absorption spectra of CsI(Tl) for the case of 80kVp x-ray with CsI(Tl) thickness of 100$\mu$m and 600$\mu$m. With a thin CsI(Tl), low energy portion of the input x-ray spectrum is mainly absorbed and many of the characteristic x-rays generated following the photoelectric absorption escape from the scintillator, hence absorption efficiency and average absorbed energy are low. As the CsI(Tl) thickness increases, however, higher energies of the input x-ray spectrum also contribute to the absorption and more characteristic x-rays of CsI(Tl) are reabsorbed and both absorption

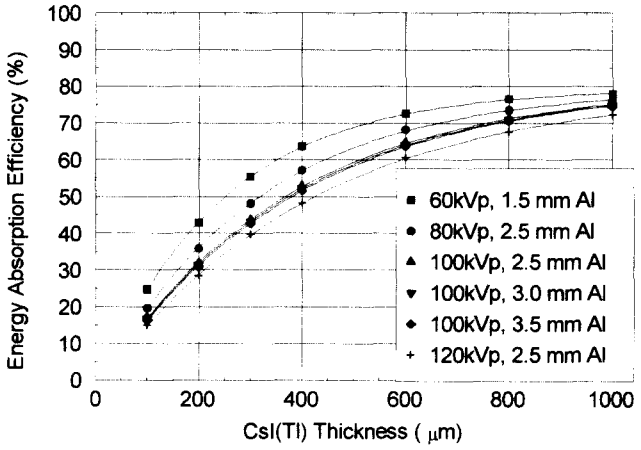


그림 5. CsI(Tl)의 에너지흡수효율
Fig. 5. Energy absorption efficiency of CsI(Tl)

efficiency and average absorbed energy increase as shown in Fig. 4. The effect of CsI(Tl) thickness on the energy absorption efficiency is shown in Fig. 5 for various x-rays. For the usual CsI(Tl) thickness of 300$\mu$m~500$\mu$m, the energy absorption efficiency is in the range of 40%~70%, which is lower than the corresponding quantum detection efficiency. Even for the 60 kVp x-rays it needs more than 1mm of CsI(Tl) thickness to absorb 80% of the input x-ray energy, which will, however, deteriorate the resolution of the imager. Therefore, there is a tradeoff between sensi-

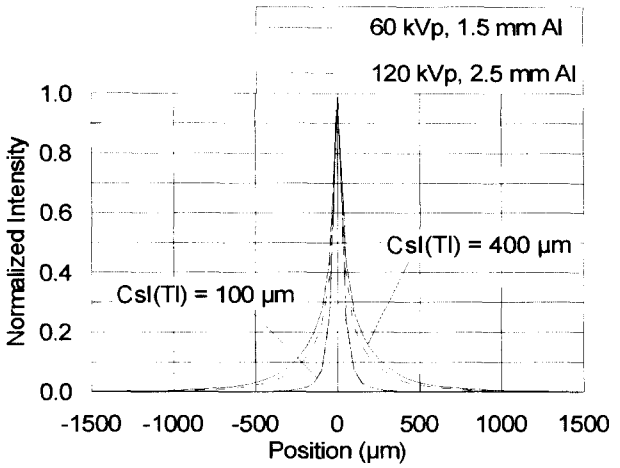


그림 6. 픽셀 크기가 50㎛인 무정형 실리콘 X-선 영상기기의 line spread functions. 해상도에 대한 CsI(Tl)의 영향이 뚜렷이 나타나 있음
Fig. 6. Line spread functions of the amorphous silicon based x-ray imager with pixel pitch of 50㎛. The effect of CsI(Tl) thickness on resolution is clearly shown

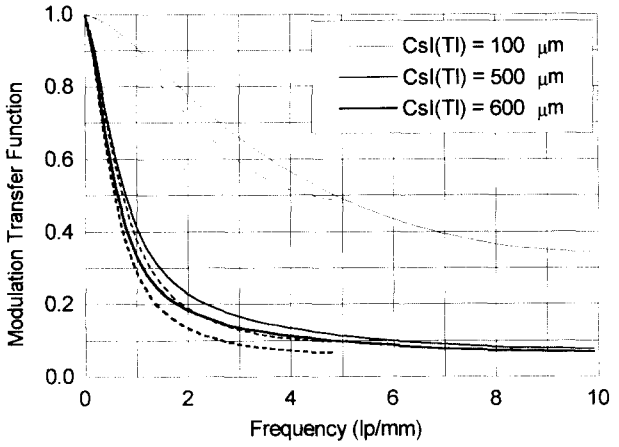


그림 7. 무정형 실리콘 X-선 영상기기의 60 kVp X-선에 대한 modulation transfer functions. 50㎛ (실선)과 100㎛ (점선)의 픽셀 크기를 사용하였음
Fig. 7. Modulation transfer functions of the CsI(Tl)/a-Si:H based x-ray imager for 60 kVp x-rays. 50㎛ (solid lines) and 100㎛ (dashed lines) of pixel sizes were used

tivity and resolution of CsI(Tl)/a-Si:H based x-ray imagers.

### 4. Spatial Resolution Analyses

The resolution of the amorphous silicon based x-ray imager is related to input x-ray energy, CsI(Tl) thickness and amorphous silicon pixel size. The line spread functions (LSF) of the imager with a pixel pitch of 50㎛ and CsI (Tl) thickness of 100㎛ and 400㎛ are shown in Fig. 6 for 60 kVp and 120 kVp x-rays. The average mean free paths of 60 kVp and 120 kVp x-rays in CsI(Tl) are about 120㎛ and 205㎛, respectively. Therefore the light generation along the passage of x-rays through 100㎛ of CsI(Tl) is almost uniform for both energies and there is little difference between the LSFs of these two energies. For 400㎛ CsI(Tl), however, due to the difference in mean free paths, light generation by 60 kVp x-rays is more concentrated in upper region of the CsI(Tl) than 120 kVp x-rays, resulting in a little wider LSF for 60 kVp x-rays. It is clearly shown in Fig. 6 that thicker scintillator produces lower resolution due to wider light spread, and the effect of scintillator thickness on the resolution is more prominent than x-ray energy.

As the energy effect on the resolution is small, different filtration of x-rays did not affect the resolution. Therefore filter thickness can be determined solely for the purpose of reducing patient dose.

Resolution study was mostly done by modulation transfer function (MTF) analyses. The MTFs we obtained from the

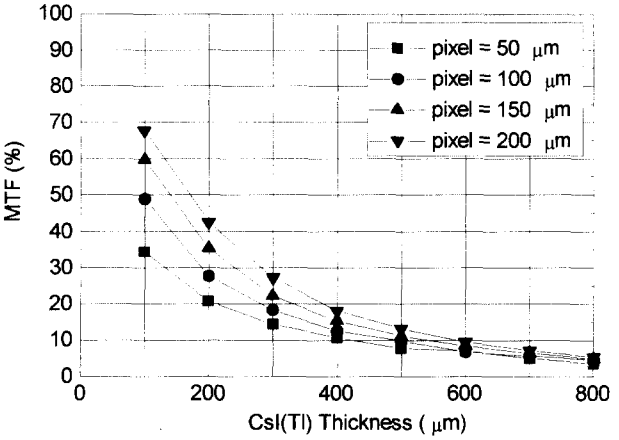


그림 8. 여러 가지 조합의 CsI(Tl) 두께와 무정형 실리콘 픽셀크기에 대한 Nyquist 주파수에서의 MTF 값
Fig. 8. MTF values at Nyquist frequencies for various combinations of CsI(Tl) thicknesses and amorphous silicon pixel sizes

simulation results were similar to the experimental measurements of other groups[4,5]. The effects of CsI(Tl) thickness and amorphous silicon pixel size on the resolution are shown in Fig. 7. With a 100㎛ thick CsI(Tl), the MTF values at Nyquist frequency is so high that the resolution is limited by pixel size. With a 500㎛ or 600㎛ thick CsI (Tl), however, the MTF values drop rapidly and at Nyquist frequencies the MTF levels are less than 10%, hence the resolution is not confined to the pixel size. A combination of 500㎛ CsI(Tl) and 100㎛ pixels shows a similar MTF

shapes to 600$\mu$m CsI(Tl) with 50$\mu$m pixels below 20% level. The system resolutions of these two combinations would be similar and using smaller pixels is not beneficial in a sense of better resolution. Therefore, there is a critical thickness of the scintillator above which the resolution is not defined by the pixel size. Fig. 8 shows the effect of pixel size and CsI(Tl) thickness on MTF values at Nyquist frequencies. This figure is useful for selecting proper combinations of CsI(Tl) thicknesses and pixel sizes. For example, if we set the lower limit of MTF values of the imager to 10% and use 100$\mu$m pixels, then up to about 500$\mu$m thick of CsI(Tl) can be used.

## CONCLUSIONS

We developed Monte Carlo simulation codes in order to quantitatively investigate sensitivity and resolution characteristics of the amorphous silicon based x-ray imager. Our simulation results were in agreement with experimental measurements reported by other groups. In the simulations we tested various combinations of x-ray qualities, scintillator thicknesses and sizes of amorphous silicon pixel diodes, which would require significant effort and time if done by experimental measurements.

Quantum detection efficiencies for 60 kVp~120 kVp x-rays with 300$\mu$m~500$\mu$m CsI(Tl) scintillator were in the range of 70%~95%, while energy absorption efficiencies were 40%~70%. Filtration of x-rays slightly affected the detection efficiencies but had no effect on spatial resolutions. The x-ray energy had little effect on resolution with thin CsI(Tl), such as 100$\mu$m, and higher x-ray energies produced slightly better resolutions when thicker CsI (Tl) was used. Resolution was primarily determined by a combination of CsI(Tl) thickness and amorphous silicon pixel size. With a thin CsI(Tl), resolution was limited by the pixel size, whereas both of CsI(Tl) thickness and pixel size were important when a thick CsI(Tl) was used.

From our simulations, we could provide proper combinations of CsI(Tl) thickness and pixel size with which detection efficiency and resolution can be optimized. These values can be used as references when designing optimum performance amorphous silicon based x-ray imagers.

## ACKNOWLEDGMENT

This paper was supported by NON DIRECTED RESEARCH FUND, Korea Research Foundation, 1996.

## REFERENCES

1. I. Fujieda, S. Nelson, P. Nylen, R. A. Street, and R. L. Weisfield, *"Two operation models of 2D a-Si sensor arrays for radiation imaging,"* J. Non-Crystal. Solids, vol. 137&138, pp.1321-1324, 1991.
2. L. E. Antonuk, J. Yorkston, W. Huang, J. Boudry, and E. J. Morton, *"Large area, flat-panel a-Si:H arrays for x-ray imaging,"* SPIE Proceedings, vol. 1896, pp.18-29, 1993.
3. H. K. Lee, J. S. Drewery, W. S. Hong, T. Jing, S. N. Kaplan, et al., *"Hydrogenated amorphous silicon (a-Si:H) based gamma camera - Monte Carlo simulations,"* SPIE Proceedings, vol. 2163, pp.427-438, 1994.
4. J. Chabbal, C. Chaussat, T. Ducourant, L. Fritsch, J. Michailos, et al., *"Amorphous silicon x-ray image sensor,"* SPIE Proceedings, vol. 2708, pp.499-510, 1996.
5. T. Graeve, Y. Li, A. Fabans, and W. Huang, *"High-resolution amorphous silicon image sensor,"* SPIE Proceedings, vol. 2708, pp.494-498, 1996.
6. H. K. Lee, G. Cho, J. S. Drewery, W. S. Hong, T. Jing, et al., *"New a-Si:H photo-detectors for long-term charge-storage,"* Mat. Res. Soc. Symp. Proceedings, vol. 297, pp.1023-1028, 1993.
7. I. Holl, E. Lorenz, and G. Mageras, *"A measurement of light yield of common inorganic scintillators,"* IEEE Trans. Nucl. Sci., vol. 35, pp.105-109, 1988.
8. I. Fujieda, G. Cho, J. S. Drewery, T. Gee, T. Jing, et al., *"X-ray and charged particle detection with CsI(Tl) layer coupled to a-Si:H photodiode layers,"* IEEE Trans. Nucl. Sci., vol.38, p.255-262, 1991.
9. L. E. Antonuk, J. Boudry, Y. El-Mohri, W. Huang, J. Siewerdsen, et al., *"A high resolution, high frame rate, flat-panel TFT array for digital x-ray imaging,"* SPIE Proceedings, vol. 2163, pp.118-128, 1994.
10. J. Yorkston, L. E. Antonuk, W. Huang, and R. A. Street, *"Photoresponse linearity of a-Si:H imaging pixels,"* Mat. Res. Soc. Symp. Proceedings, vol. 297, pp.951-956, 1993.
11. L. E. Antonuk, J. Yorkston, W. Huang, J. Siewerdsen, and R. A. Street, *"Considerations for high frame rate operation of two-dimensional a-Si:H imaging arrays,"* Mat. Res. Soc. Symp. Proceedings, vol. 297, pp.945-950, 1993.
12. I. Fujieda, R. A. Street, R. L. Weisfield, S. Nelson, P.

Nylen, et al., "*High sensitive readout of 2D a-Si image sensors,*" Jpn. J. Appl. Phys., vol. 32, pp.198-204., 1993.
13. E. F. Plechaty, D. E. Cullen and R. J. Howerton, "*Tables an graphs of photon interaction cross sections from 1.0 keV to 100 MeV derived from the LLL evaluated nuclear data library,*" UCRL-50400, vol.6 Revision 1, 1975.
14. W. H. Press, S. A. Teukolsky, W. T. Vetterling, and B. P. Flannery, *Numerical recipes in C*, Cambridge, Cambridge University Press, pp. 274-286, 1995.
15. H. E. Johns and J. R. Cunningham, *The Physics of Radiology*, Springfield, Charles C Thomas, pp.62-64, 1983.
16. R. D. Evans, *The Atomic Nucleus*, New York, McGraw-Hill, pp. 683-690, 1955.
17. I. Lux, and L. Koblinger, *Monte Carlo particle transport methods: neutron and photon calculations*, Boca Raton, CRC Press, pp. 43-69, 1991.
18. Birch, Marshall, and Arden, "*Catalogue of Spectral Data for Diagnostic X rays,*" Hospital Physicists Association Scientific Report Series-30.